CrossMark

Capillary-Driven Transport of Dissolved Salt to the Drying Zone During CO$_2$ Injection in Homogeneous and Layered Porous Media

Saskia M. Roels[1] · **Ntiana El Chatib**[1] · **Costas Nicolaides**[1] ·
Pacelli L. J. Zitha[1]

Abstract A major challenge of CO$_2$ injection into saline aquifers is the risk of formation clogging due to salt precipitation. Capillary-driven flow of brine can provide a continuous transport of dissolved salt toward the dry zone around the injection well where it ultimately precipitates due to evaporation. In this study, core flooding experiments were performed in homogeneous coarse-textured cores and in layered cores consisting of a coarse-textured layer overlying a fine-textured layer. CO$_2$ was injected through a well in the upper part of the cores, and the bottom parts functioned as brine sources. Impairment in injectivity was found due to accumulation of precipitated salt caused by capillary-driven flow from the brine sources to the upper dryer region. Compared to flow domains without a brine source, we found that capillary-driven upward flow at first prevents complete clogging because the porous medium remains wet, but eventually leads to a more severe clogging of the entire domain. The results show that after sufficient dry-out, a coarse-textured injection layer can draw brine from an underlying fine-textured layer by capillary forces. A connected fine-textured layer can therefore contribute to salt precipitation and clogging of the injection layer.

Keywords CO$_2$ sequestration · Salt precipitation · Core flooding · Capillary-driven flow

1 Introduction

Formation clogging during CO$_2$ injection caused by precipitation of salt can decrease storage potential substantially. Reduced storage capacity can occur by (1) a decrease in available pore space caused by the presence of solid salt (e.g., Bacci et al. 2011; Hurter et al. 2007; Pruess and Müller 2009) and (2) complete clogging of the porous medium in the vicinity of the injection well by solid salt accumulation (e.g., Giorgis et al. 2007; Muller et al. 2009; Peysson et al. 2014). Whether salt precipitation will affect the injectivity depends on its distribution inside

---

✉ Saskia M. Roels
saskiaroels@hotmail.com

[1] Delft University of Technology, Stevinweg 1, 2628 CN Delft, The Netherlands

the porous medium. In case viscous forces dominate over capillary forces, salt precipitates locally, and the decrease in soil permeability due to salt precipitation can be counteracted by the increase in relative permeability caused by the increase in CO_2 saturation (Ott et al. 2011; Roels et al. 2014). When capillary forces are dominant over viscous forces, complete clogging can occur by accumulation of salt via continuous transport of brine by capillary forces toward to the dry zone around the injection well (Alkan et al. 2010; Peysson 2012).

Capillary-driven flow of brine occurs due to a gradient in brine saturation, which can be established by evaporation. Evaporation of water from the formation brine into the injected CO_2 is a complex phenomenon: It occurs due to the mutual solubility of CO_2 and water (Spycher and Pruess 2005, 2010). The rate of evaporation depends on factors including interfacial area between brine and CO_2 (Niessner and Hassanizadeh 2009), persistence of liquid pathways to supply brine to the drying front (Lehmann et al. 2008; Nachshon et al. 2011; Shokri et al. 2010), CO_2 flow velocity (Zuluaga et al. 2001) and thermodynamic properties which determine the vapor pressure. The efficiency of evaporation determines the steepness of the gradient in brine saturation inside the porous medium and therefore the significance of capillary-driven flow.

Recently, we have shown that at high CO_2 injection velocities, the assumption of local equilibrium for evaporation leads to an overestimation of salt accumulation near the inlet (Roels et al. 2014). Controlled μ-CT scan experiments showed that solid salt was uniformly distributed inside the porous medium after complete dry-out and impairment in injectivity was not found. The findings were supported by numerical simulation including a kinetic phase partitioning between brine and CO_2. This suggested that injection velocity plays a major role in the potential of clogging. At high injection velocities, CO_2 does not become saturated with water vapor, and evaporation takes place throughout the whole domain. Brine saturation decreases gradually in the entire domain, and capillary-driven backflow does not occur. Similar results were found by André et al. (2014) and Peysson et al. (2014) where capillary-driven backflow was limited above a threshold gas injection rate, and salt accumulation near the inlet was only found for low injection velocities. The threshold value of the injection rate was found to depend on the salinity of the brine.

Potential CO_2 injection sites consist of a high-permeable, coarse-textured injection layer confined by low-permeable, fine-textured layers (aquitards) (Hosa et al. 2011). Brine inside the low-permeable, fine-textured layer is retained at the interface between the fine and coarse layers (within the fine-textured layer) by capillary forces. When the entry pressure for gas of the fine-textured layer is reached (i.e., until the entry pressure for brine for the coarse layer is reached), gas and water redistribute between the layers until equilibrium pressure is established (Schroth et al. 1998). This suggests that when the entry pressure is overcome, brine from the fine-textured layer is transported to the drying zone where it contributes to formation clogging. A capillary pressure jump between fine and coarse layers followed by a relaxation through water redistribution was also reported by Shokri et al. (2010). In addition, flow from micro-pores to macro-pores was observed in a dual-porosity system (Ott et al. 2013). The micro-porous volume functions as a brine reservoir and gradually transports dissolved salt to the macro-porous channels as dry-out proceeds.

The primary goal of the present study was to investigate permeability impairment due to salt accumulation induced by capillary-driven flow of brine, accounting for connected brine sources. CO_2 injection experiments were performed to investigate brine redistribution dynamics during dry-out of a porous medium. Capillary-driven flows and the resulting permeability impairment were examined for isolated porous media and media in contact with a source of brine. The effect of capillary suction from a fine-textured layer to a coarse- textured layer was studied using a layered porous medium. The following section discusses
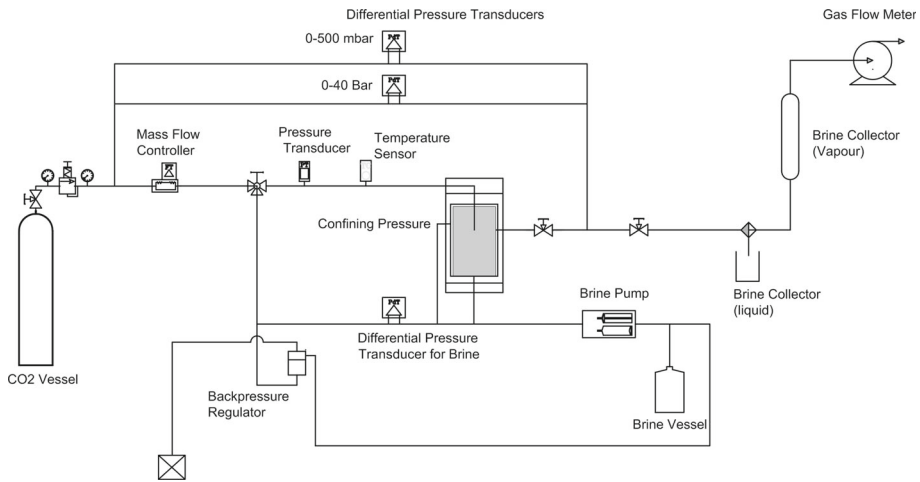
Fig. 1 Experimental setup for radial core flooding

experimental details on the core floods. After that, the experimental results are presented and evaluated using fundamental principles on dry-out during two-phase flow. Concluding remarks on the potential of formation clogging and the influence of capillary-driven flow on solid salt distribution are presented in the last section.
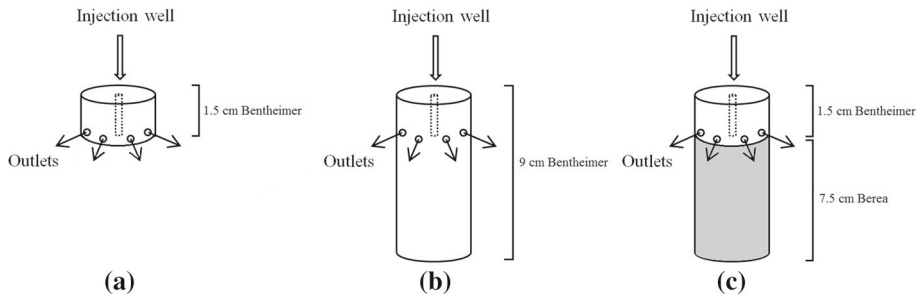
2 Core Flooding Experiments

2.1 Experimental Set-Up

The experimental set-up used in this study is shown in Fig. 1. CO_2 with 99.7 % purity was supplied from a pressurized vessel using a Bronkhorst EL-FLOW® mass flow controller. Brine solution was injected by a P-500 Pharmacia Biotech pump. During CO_2 injection, two pressure transducers (range 0–500 mbar and 0–40 bar) were used to accurately measure the pressure drop during brine displacement as well as during the dry-out phase. A third pressure transducer (range 0–40 bar) was used during brine filling. Inlet temperature was measured using a two-wire thermocouple with an accuracy of 0.1 °C. A data acquisition system was used to monitor the measuring devices (National Instruments). The amount of produced water vapor in the CO_2 phase was measured by connecting the outlet to a cooling bath of 2.5 °C, in which the water vapor condensed. The remaining produced volume of CO_2 was measured by a gas meter (RITTER MilliGascounter).

2.2 Porous Media and Brine

The first set of experiments were performed with a cylindrical macroscopically homogeneous Bentheimer sandstone core of 4 ± 0.1 cm diameter and 1.5 ± 0.1 cm height (Fig. 2a). In the second sets of experiments, Bentheimer sandstone core of 4 ± 0.1 cm diameter and 9 ± 0.1 cm height was used (Fig. 2b). The third set of experiments was performed on a layered system, formed by an upper layer consisting of Bentheimer sandstone and bottom layer consisting of Berea sandstone. The sandstone samples had both diameter 4 ± 0.1 cm diameter and

Fig. 2 Schematics of cores used for the flooding experiments with **a** short Bentheimer core, **b** long Bentheimer core, and **c** layered core of Bentheimer and Berea. The bottom part of **b** and **c** function as brine sources for capillary-driven flow

Table 1 Sandstone properties and parameters

Property	Bentheimer	Berea	Unit
Porosity	0.21 ± 0.01	0.21 ± 0.01	–
Permeability	$1.3 \pm 0.1 \times 10^{-12}$	$2.4 \pm 0.1 \times 10^{-13}$	m^2
P_d—Van Genuchten	3.3×10^4	6.0×10^4	Pa
m—Van Genuchten	0.85	0.9	–

heights 1.5 ± 0.1 and 7.5 ± 0.1 cm, respectively (Fig. 2c). The cores were completely sealed with epoxy glue to avoid bypassing of the injected liquids. An injection well of 4 mm diameter and 1.5 cm depth was drilled from the top in the middle of the core. Eight outlets symmetrically distributed around the core were drilled in the epoxy layer in order to establish quasi-radial flow conditions. The properties of the cores are listed in Table 1. The capillary pressure parameters for Bentheimer were obtained by fitting the Van Genuchten equation (Van Genuchten 1980) to the capillary pressure data measured by mercury injection (Roels et al. 2014). For Berea, we used capillary pressure parameters obtained from Berg et al. (2013) for a Berea sandstone with similar permeability. The cores were placed into a polyether ether ketone (PEEK) core holder which was specially designed and built to cope with the requirements for radial flow. The core holder was placed inside a third-generation Siemens SOMATOM CT scanner for 3D imaging of the rock matrix and the fluid distribution in it. Brine consisting of nearly saturated potassium iodide (KI) solution (58.3 wt%) was used to conduct the experiments. KI has high X-ray attenuation coefficient due to its high density and mass number and enhances the contrast between the CO_2 and brine. In this way, optimal CT scanning results were obtained.

2.3 Experimental Procedure

Table 2 gives an overview of the steps taken during the experiments. Air was removed from the core by flushing it with CO_2 for several hours at ambient temperature and pressure. Next, the core was saturated with brine from bottom to top at 2.5 mL/min for 3 h. Then, the back pressure was increased to 25 bar and brine injection continued at 1 mL/min for another 2 h to ensure that any remaining CO_2 was dissolved. CT scans were taken to check that complete brine saturation was established. After that, the pressure was slowly decreased to

Table 2 Experimental procedure used to perform core flooding experiments

Step	Description	Flow rate	Back pressure (bar)	Duration (h)
1	CO_2 flushing	–	1	3
2	CT scan (dry)	–	–	–
3	Brine filling	2.5 mL/min	1	3
4	Brine filling	1 mL/min	25	2
5	Brine filling	2.5 mL/min	1	2
6	CT scan (brine)	–	–	–
7	CO_2 injection	15 NmL/min	1	144
8	CT scans	–	–	–

atmospheric pressure while continuing brine injection with 2.5 mL/min for another 2 h. After completion of the core saturation with brine, CO_2 injection was initiated with 15 NmL/min, corresponding to injection of 1 Mt/year in an aquifer of 100 m thickness under 45 °C and 100 bar. Pressure and pressure drop were monitored continuously and captured every 10 s by a data acquisition system. The entire experiment was performed at ambient temperature which was monitored using a two-wire thermocouple with an accuracy of 0.1 °C. Injection of CO_2 would be terminated when only minor changes in pressure drop would be observed for a long period of time (± 0.5 bar), when the maximum safety pressure of 20 bar would be reached or when the maximum duration of the experiment of 6 days would be reached. To ensure reproducibility, the experiments were carried out in duplicate.

2.4 CT Scanning

The saturation distribution inside the porous medium was monitored by taking CT scans every few hours. Four slices were taken near the center of the core, each consisting of 512×512 pixels with the pixel size of 0.3×0.3 mm. The noise for CT images typically ranges from 3 to 20 Hounsfield Units (HU), corresponding to an accuracy of $\pm 2\%$ (Simjoo et al. 2012). CT scans produce images consisting of voxels with a Hounsfield Unit (HU) according to the average saturation inside the voxel, with a higher HU corresponding to a higher density. The HU for CO_2 at the experimental pressure and temperature is close to the value of air, which is -1000. KI solution has a value of approximately 3000, which is close to the maximum value of the HU scale (3071). Since solid salt has an even higher density than brine, its phase cannot be distinguished from brine. Therefore, in the CT images, brine and solid salt were treated as a single phase. The files were imported into and processed in MATLAB® to calculate brine saturations at different time steps (Akin and Kovscek 2003; Simjoo et al. 2012). When imported into MATLAB® for processing, the values are stored as HU+1024 in order to do calculations.

To visualize the distribution of solid salt inside the core, μ-CT scans were taken at the end of the experiment. The core was removed from the core holder and scanned in the μ-CT scanner, with resolution of $22 \times 22 \times 22$ μm. The μ-CT images were reconstructed with the Phoenix reconstruction software which is based on the Feldkamp algorithm (Feldkamp et al. 1984), after which the resolution of the images was decreased to $43 \times 43 \times 43$ μm, in order to obtain a workable file size.

3 Results and Discussion

In the following sections, the experimental results are presented and discussed. In-depth analysis of driving forces of salt accumulation is described for dry-out of porous media with and without a brine source. At first, the results of CO_2 injection into a radial domain from are presented as a baseline for dry-out without connected brine source. After that, we discuss the experimental results from present study, followed by a comparison of the effect of salt precipitation on injectivity.

### 3.1 Porous Media Dry-Out and Capillary-Driven Backflow: Short Core

Figure 3 shows the CT scans for CO_2 injection into a radial domain without brine source. The first two scans which were taken at 0.6 min and 1 min after injection started show the displacement of brine by CO_2. Due to the poor mobility ratio, a high remaining brine saturation is present inside the core after CO_2 breakthrough. After breakthrough of CO_2, the main drying mechanism is evaporation of water into the gaseous phase. After 15.5 h of injection, complete clogging of the injection well was observed (dark red color). The images indicate that capillary-driven backflow of brine in combination with continuous evaporation resulted in a complete clogging of the porous medium in the vicinity of the injection well.

The potential of formation clogging due to capillary-driven backflow depends strongly on the saturation gradient inside the porous medium. We analyze the situation at which capillary-driven backflow becomes dominant over viscous-driven flow with a 1D example (Fig. 4). In the absence of gravity and compressibility, the velocity of the water phase can be described by the fractional flow formulation:

$$u_w = u_t f_w = u_t \left[\frac{\lambda_w}{\lambda_w + \lambda_g} \left(1 + \frac{\lambda_g}{u_t} \left(\frac{dP_c}{dS_w} \frac{\partial S_w}{\partial x} \right) \right) \right] \tag{1}$$

where u_w is the Darcy velocity for water, f_w is the fractional flow for water, u is the total velocity, $\lambda_g = K k_{rg}/\mu_g$ is the gas mobility and $\lambda_w = K k_{rw}/\mu_w$ is the water mobility, P_c is the capillary pressure and S_w is the water/brine saturation. The equation consists of a viscous flow term and a capillary flow term, where the derivative dP_c/dS_w is negative and the direction of brine flow is determined by the dominancy of either viscous or capillary-driven flow.

In Fig. 4, the viscous flow velocity is represented by the dashed line and the capillary flow velocity is shown in solid black lines, for $\partial S_w/\partial x$ is 0, 2, 4, 6, 8 m^{-1}. The highest value for $\partial S_w/\partial x$ is represented by the first solid line from the left. Less steep slopes of $\partial S_w/\partial x$ result in a lower capillary-driven flow velocity. The viscous flow velocity is constant for all cases. The red lines represent u_w, being the sum of the viscous flow velocity and the capillary flow velocity. The first red line from the top corresponds to the highest value for $\partial S_w/\partial x$. For experimental conditions, the capillary-driven term has the highest (negative) velocity for a
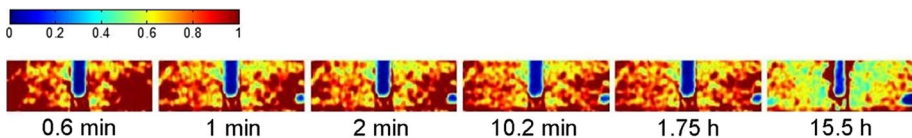
Fig. 3 Brine saturation at different times obtained from CT scan imaging. The brine saturation represents both the presence of brine and solid salt. After 15.5 h of injection, complete clogging of the injection well can be observed (*dark red*)
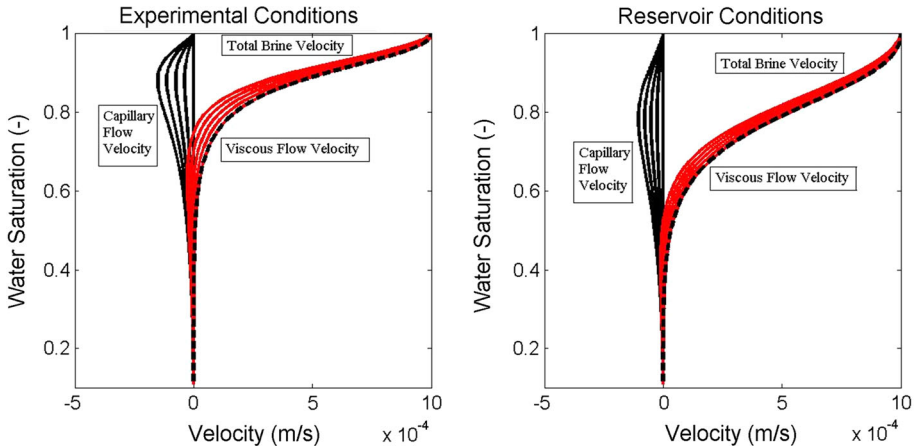
Fig. 4 Comparison of viscous flow velocity and capillary flow velocity at experimental and reservoir conditions. The total brine velocity, u_w, is represented by the red lines and consists of the sum of the viscous and capillary flow velocities. Capillary flow velocity is plotted versus saturation for $\partial(S_w, x)$ varying from 1 (closest to the y-axis) to 8 (furthest from the y-axis) m^{-1}. Below a certain water saturation, the value of the capillary flow velocity exceeds the viscous flow velocity and u_w becomes negative

water saturation of approximately 0.85. The unfavorable mobility ratio for brine displacement by CO_2 under experimental conditions stimulates the term for capillary-driven backflow at high water saturations. For comparison, we show the potential for backflow of brine under reservoir conditions, 45 °C/100 bar. The ratio between gas and water mobility is lower, and therefore the capillary-driven term becomes dominant at a lower water saturation. The viscous flow term is also affected by a lower mobility ratio so that the viscous velocity is higher for the same water saturation. The red lines show that at a certain water saturation, capillary-driven flow exceeds viscous flow, and backflow of brine toward the injection point occurs. For example, for $\partial S_w/\partial x = 8$ m^{-1}, capillary-driven backflow dominates over viscous-driven flow below a water saturation of approximately 0.75 and 0.55 for experimental and reservoir conditions, respectively.

3.2 In Situ Brine Saturation Redistribution During Dry-Out: Long Cores

Brine saturation distributions were calculated from the CT scans at various times during CO_2 injection into the Bentheimer sandstone core and the layered core consisting of Bentheimer and Berea (Fig. 5). The first scans from the left-hand side which were taken at 1 min and 10 min after CO_2 injection started show the remaining brine saturation after CO_2 breakthrough. The scans show that in both systems CO_2 initially does not propagate into the lower part of the cores. In particular in the layered system, it is clearly visible that Berea layer does not get penetrated by CO_2 at all. As injection continues, after approximately 98 h, dry-out of the lower parts of the cores become visible and is more pronounced in the homogeneous Bentheimer system. At 142 h, dry-out of the lower part of the Berea sandstone has become significant.

Solid salt could not be quantified directly from the CT scans, but the results indicate that salt precipitation takes place throughout the whole upper part in case of the Bentheimer core. Salt precipitation is observed only near the top in the layered system (dark red). For the latter system, the lower part of the Bentheimer layer seems to dry-out completely with brine
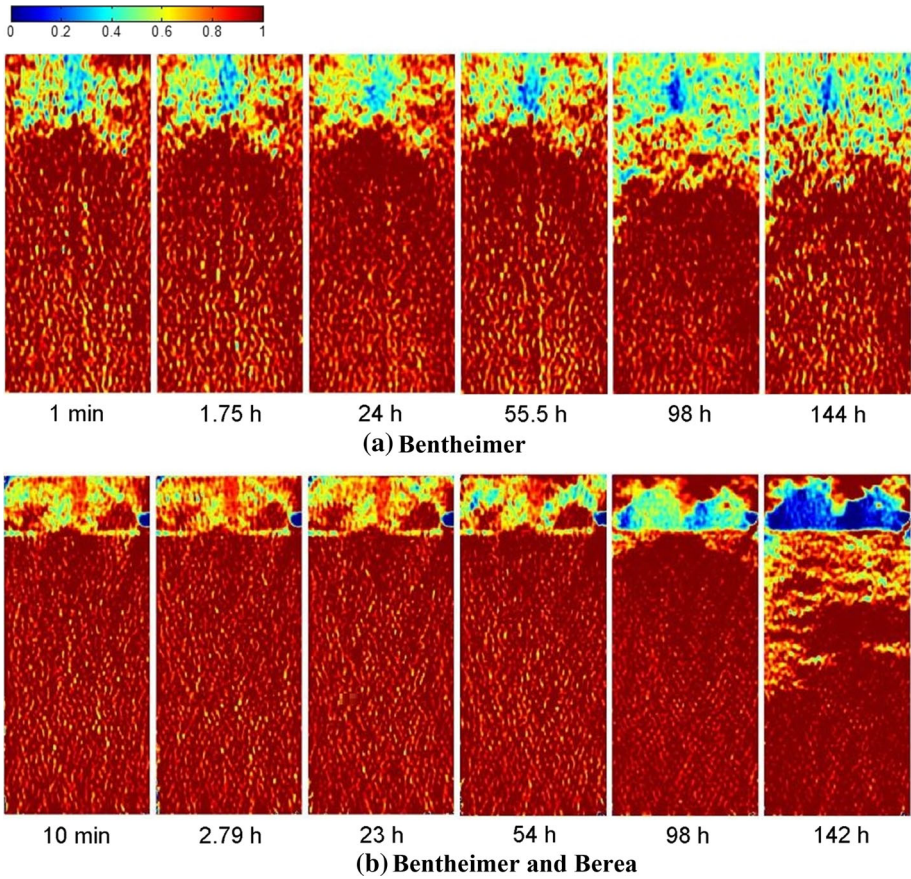
Fig. 5 CT scan images at various times for **a** homogeneous Bentheimer core and **b** layered Bentheimer and Berea core

saturations lower than 0.2 (dark blue). The physical mechanism responsible for the severe dry-out on the upper part is addressed in the next section. Complete clogging in the vicinity of the injection well as observed in previous work with a fully penetrating well in a short core (Fig. 3) did not take place.

To compare the saturation distribution inside the porous media we have averaged the values over the width of each slice and plotted against core height in Fig. 6. The black line represents the brine saturation in the homogeneous core, and the gray line represents the saturation in the layered core. After displacement and in the early stages of dry-out (the first four figures from the left), a comparable brine saturation was found in the upper part which both consist of Bentheimer. This shows that the composition of the core (homogeneous or layered) did not affect the displacement process. A difference in brine saturation between the two experiments can be observed at a height of 7–7.5 cm, with lower brine saturations in the homogeneous core and a fully saturated Berea layer in the layered core. Due to the fact that the scanned object is not symmetric in the direction of scanning and the presence of beam-hardening artifacts (the low energy and thus strongly attenuated photons are eliminated
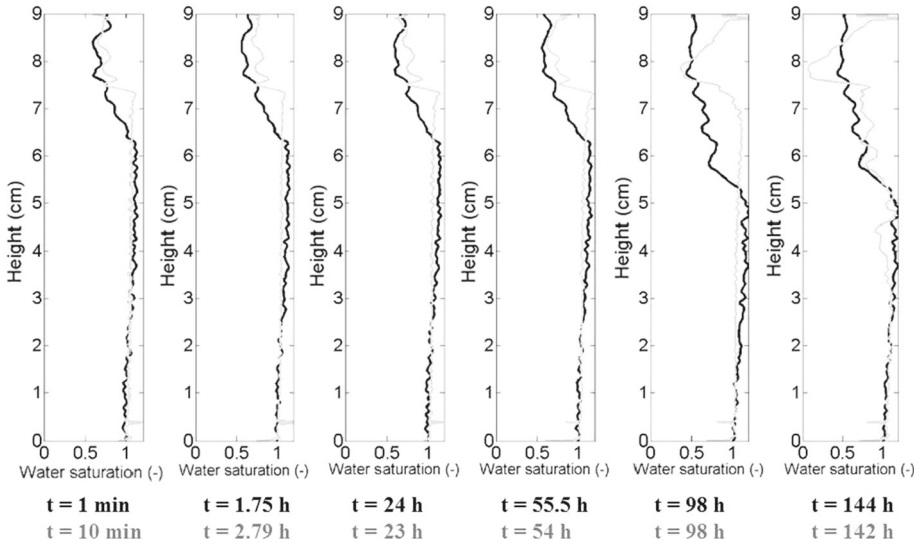
Fig. 6 Brine saturation calculated from the CT scans and averaged over the width. The *black line* represents the homogeneous core, and the *gray line* represents the layered core

from the beam at a faster rate than the higher, weakly attenuated energy levels), a saturation that slightly exceeds 1 was found for the middle part of the cores.

The fifth scan shows how dry-out starts to affect the brine saturation distribution. For the homogeneous core, we can observe a decrease in brine saturation below 6 cm height as the dry-out front propagates into the lower part. At this time, the bottom part of the layered system remains fully saturated with brine. The last scan in Fig. 6 shows how the brine saturation in the Berea layer eventually decreases as well (gray line). The upper part has eventually reached sufficiently low brine saturation values so that capillary suction from the bottom part can start taking place.

3.3 Visualization of Solid Salt by μ-CT Scans

After the core floods were terminated, μ-CT scans were taken from the short core and the layered core in order to visualize solid salt inside the porous media. Figure 7 shows slices taken at a depth of 0.8 cm from the top of the cores. After reconstruction, the color map ranges on a grayscale from black to white with increasing density. Solid salt has a high density ($3.1\,\mathrm{g/cm^3}$) and is represented by white, CO_2 has a low density ($0.0018\,\mathrm{g/cm^3}$) and is shown in black, and the porous medium has an intermediate density ($2.6\,\mathrm{g/cm^3}$) and is shown in gray. It was found by Van Hemert et al. (2013) that salt crystals tend to cover multiple connecting pore spaces and can therefore be clearly detected by the μ-CT scanner.

The images confirm that solid salt accumulated around the injection well inside the short Bentheimer core (Fig. 7a). The light gray color in the outer part of the core shows pore spaces filled with brine. This means that the injection well was completely clogged before complete dry-out was reached. A different salt pattern was observed in the layered system (Fig. 7b). Salt precipitated throughout the Bentheimer layer and reduced the available pore space dramatically.
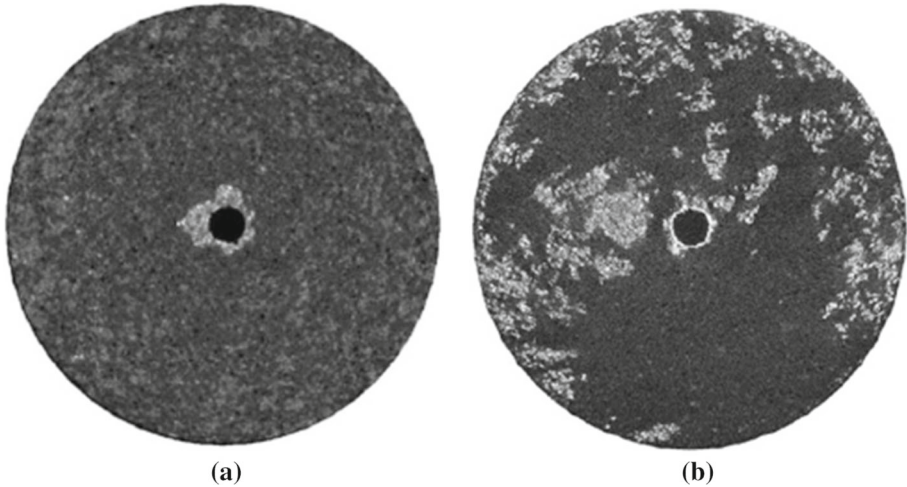
Fig. 7 Post experiment μ-CT scans taken at 0.8 cm from the *top* from **a** short Bentheimer core and **b** layered core. *White color* represents higher density (solid salt) and *black color* represents lower density (CO_2). Solid salt was found **a** accumulated around the injection well and **b** distributed along the domain

3.4 Capillary-Driven Flow Directions in Homogeneous and Layered Systems

Figure 8 shows a conceptual illustration of the brine flow regimes in the different cores resulting in different salt precipitation patterns. In the short core (Fig. 8a), brine flow is directed toward the dry zone around the well, and accumulation of salt leads to a relatively fast clogging of the porous medium in the vicinity of the injection well. When a brine source is present within a layer with equal water retention properties as the injection layer (homogenous core) (Fig. 8b), capillary-driven flow of brine from the source will continuously redistribute the brine saturation so that the zone around the well remains wet. The brine source therefore delays salt precipitation and retards accumulation near the injection well.

In case the brine source consists of a layer with stronger water retention properties than the injection layer, dry-out continues to a greater extent before redistribution of brine starts. This mechanism can be explained by Fig. 9 which shows the water retention curves for Bentheimer and Berea with the parameters from Table 1. In the homogeneous long core, the slope of the P_c (S_w) curve starts to increase as brine saturation decreases (Fig. 9, dashed line) and capillary-driven forces become stronger. As a consequence, capillary suction of brine toward the upper dry zone occurs. In the layered system, the bottom part consists of Berea and is represented by the black line. The brine saturation in the upper part decreases due to evaporation and capillary pressure becomes higher. At a certain saturation, the capillary pressure equals the entry pressure of the lower region (arrow). As dry-out continues, the system will redistribute its fluids in such way that the difference in capillary pressure at the contact area is minimized. However, if the upper layer reaches complete dry-out at a capillary pressure that is lower than the pressure that needs to be overcome to redistribute the brine between the low- and high-permeable layer, the influence of additional salt precipitation will be minimal.
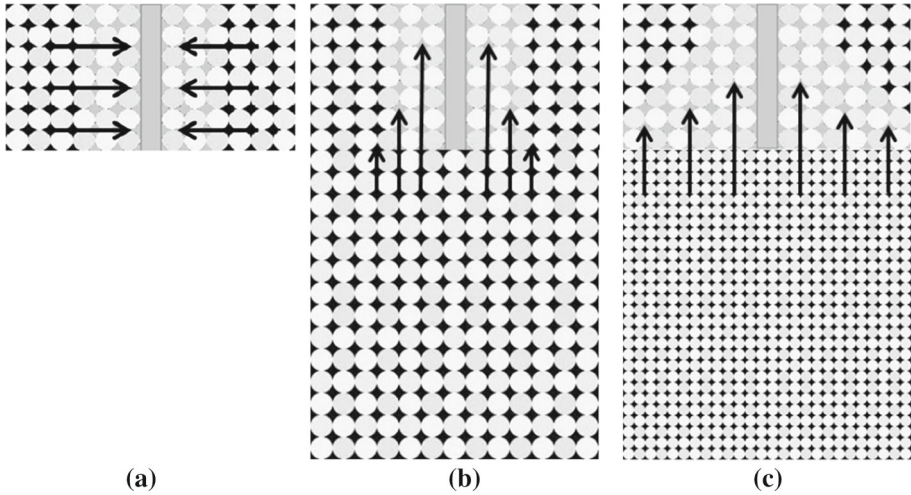
Fig. 8 Conceptual illustration of capillary suction of brine toward the dry zone for **a** without brine source, **b** with homogeneous system and **c** layered system

Fig. 9 Capillary pressure water saturation curves for Bentheimer (*dashed line*) and Berea (*solid line*). After sufficient dry-out, fluid will be redistributed so that capillary pressure equilibrium is maintained between Bentheimer and Berea
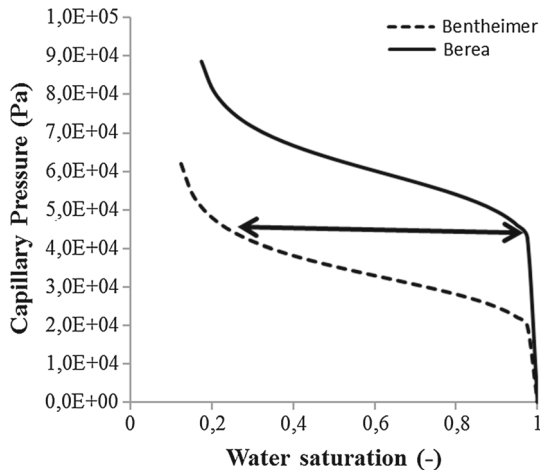
3.5 Effect of Salt Precipitation on Pressure Drop

The pressure drop between injection well and outlets measured during the experiments is shown in Fig. 10. The dashed line shows the pressure drop from the experiment with the short radial core. In that experiment, the maximum safety pressure is reached within approximately 15 h. The pressure drop during CO_2 injection into the long Bentheimer core is represented by the black line and the line with symbols shows the pressure drop in the layered core. All systems show an increase in pressure drop due to a decrease in soil permeability caused by the precipitation of salt. The pressure drop increases gradually for systems in which a brine source was included at the bottom, whereas in the absence of a brine source, clogging occurred much faster.
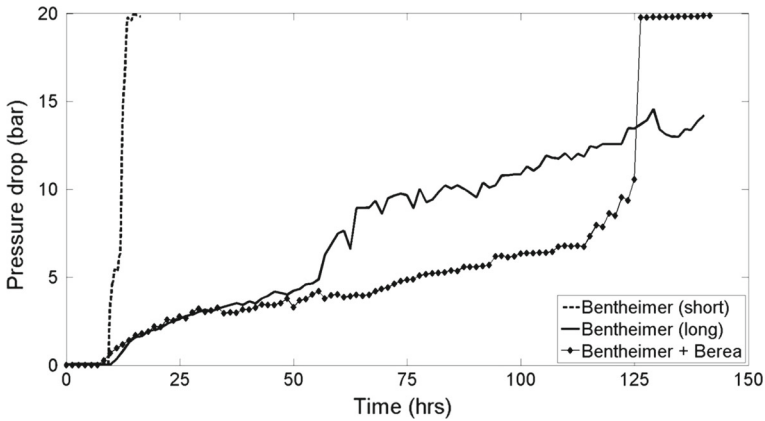
Fig. 10 Pressure drop vs. time for three experiments. The *dashed line* represents the short Bentheimer core, the *black line* represents the long Bentheimer core and the *line with symbols* represents the layered core of Bentheimer and Berea. Salt precipitation lead to an increase in injection pressure in all cases

The results indicate that the brine source delays salt precipitation by keeping the porous medium wet for a longer period of time. It was found in the CT scans that salt accumulated around the well in absence of a brine source, whereas more salt precipitation throughout the domain was found in presence of a brine source. This indicates that capillary-driven flow toward the well, i.e., a brine saturation gradient created by evaporation, is stronger in the short core. The presence of a brine source prevents the establishment of a saturation gradient between injection well and outlet, but rather establishes a gradient between upper and lower part of the cores. This is consistent with the conceptual model given in Fig. 8.

3.6 Implications for Field Scale Injection

An important factor that influences the amount of pore volume that will be blocked by the precipitation of solid salt is the amount of dissolved salt available in the brine after displacement. In case of KI solution, which has a high solubility limit, the concentration of dissolved salt is high and therefore a significant impact on permeability impairment can be expected. A brine solution with smaller concentration of dissolved salt, as well as solutions with types of salt with lower solubility limit (e.g., NaCl solutions and formation brine), will show similar precipitation patterns but with smaller volume of occupied pore space, and therefore a smaller impact in pressure drop.

On the other hand, the amount of brine available for capillary-driven flow in the experiments is limited, whereas under field conditions the source of brine is 'unlimited.' The brine source in the injection layer as well as in the less permeable confining layer(s) could provide flow of brine toward the injection well until complete clogging has been reached. In contrast, in Fig. 4, we showed that the potential for backflow of brine under reservoir conditions, 45 °C/100 bar, is lower than under current experimental conditions. Under reservoir conditions, the ratio between gas and water mobility is lower, and therefore the capillary-driven term is less pronounced. However, field scale scenarios have been studied numerically (e.g., Giorgis et al. 2007; Muller et al. 2009; Peysson et al. 2014) and have shown that under reservoir conditions, capillary-driven backflow can be strong enough to cause severe injection impairment due to formation clogging in the vicinity of the well.

4 Summary and Conclusions

Radial CO_2 injection core flooding experiments were performed in a homogeneous and a layered system, both containing a brine source. The results were compared with previous work without a brine source and the effect of capillary suction on formation clogging was studied. CT scans were taken to quantify the saturation distributions inside the porous medium at various times during dry-out. The effect of salt precipitation on injectivity was measured by monitoring the pressure drop over the core while injecting CO_2.

Experimental evidence indicates that formation clogging due to salt precipitation during CO_2 injection forms a substantial risk. It was found that capillary rise from a brine source toward the drying zone retards complete impairment injectivity by keeping the porous medium wet. However, continuous transport of brine to the injection zone eventually decreases the permeability of the porous medium dramatically and injection pressure rises.

For a coarse-textured layer overlying a fine-textured layer, it was found that capillary suction into the coarse layer starts when the layer is sufficiently dry. Tendency toward equilibrium in capillary pressure between the two layers leads to a continuous redistribution of brine inside the layered system. The results show that during CO_2 injection into a coarse sandstone layer, dry-out can lead to brine suction from a connecting fine sandstone layer. Transport of brine from the fine-textured layer can contribute to accumulation of salt and severe clogging of the injection layer. Current study shows that formation clogging due to salt precipitation during CO_2 injection can be underestimated when connected layers are not taken into account.

References

Akin, S., Kovscek, A.: Computed tomography in petroleum engineering research. Geol. Soc. Lond. Spec. Publ. **215**, 23–38 (2003)

Alkan, H., Cinar, Y., Ülker, E.: Impact of capillary pressure, salinity and in situ conditions on CO_2 injection into saline aquifers. Transp. Porous Media **84**, 799–819 (2010)

André, L., Peysson, Y., Azaroual, M.: Well injectivity during CO_2 storage operations in deep saline aquifers-Part 2: Numerical simulations of drying, salt deposit mechanisms and role of capillary forces. Int. J. Greenh. Gas Control **22**, 301–312 (2014)

Bacci, G., Korre, A., Durucan, S.: Experimental investigation into salt precipitation during CO_2 injection in saline aquifers. Energy Procedia **4**, 4450–4456 (2011)

Berg, S., Oedai, S., Ott, H.: Displacement and mass transfer between saturated and unsaturated CO_2-brine systems in sandstone. Int. J. Greenh. Gas Control **12**, 478–492 (2013)

Feldkamp, L., Davis, L., Kress, J.: Practical cone-beam algorithm. JOSA A **1**, 612–619 (1984)

Giorgis, T., Carpita, M., Battistelli, A.: 2D modeling of salt precipitation during the injection of dry CO_2 in a depleted gas reservoir. Energy Convers. Manag. **48**, 1816–1826 (2007)

Hosa, A., Esentia, M., Stewart, J., Haszeldine, S.: Injection of CO_2 into saline formations: benchmarking worldwide projects. Chem. Eng. Res. Des. **89**, 1855–1864 (2011)

Hurter, S., Berge, J.G., Labregere, D.: Simulations for CO_2 injection projects with compositional simulator. Offshore Europe (2007)

Lehmann, P., Assouline, S., Or, D.: Characteristic lengths affecting evaporative drying of porous media. Phys. Rev. E **77**, 056309 (2008)

Muller, N., Qi, R., Mackie, E., Pruess, K., Blunt, M.J.: CO_2 injection impairment due to halite precipitation. Energy Procedia **1**, 3507–3514 (2009)

Nachshon, U., Weisbrod, N., Dragila, M.I., Grader, A.: Combined evaporation and salt precipitation in homogeneous and heterogeneous porous media. Water Resour. Res. **47** (2011)

Niessner, J., Hassanizadeh, S.M.: Modeling kinetic interphase mass transfer for two-phase flow in porous media including fluid-fluid interfacial area. Transp. Porous Media **80**, 329–344 (2009)

Ott, H., de Kloe, K., Marcelis, F., Makurat, A.: Injection of supercritical CO_2 in brine saturated sandstone: pattern formation during salt precipitation. Energy Procedia **4**, 4425–4432 (2011)

Ott, H., Snippe, J., de Kloe, K., Husain, H., Abri, A.: Salt precipitation due to Sc-gas injection: single versus multi-porosity rocks. Energy Procedia **37**, 3319–3330 (2013)

Peysson, Y.: Permeability alteration induced by drying of brines in porous media. Eur. Phys. J. Appl. Phys. **60**, 24206 (2012)

Peysson, Y., Andre, L., Azaroual, M.: Well injectivity during CO_2 storage operations in deep saline aquifers-Part 1: Experimental investigation of drying effects, salt precipitation and capillary forces. Int. J. Greenh. Gas Control **22**, 291–300 (2014)

Pruess, K., Müller, N.: Formation dry-out from CO_2 injection into saline aquifers: 1. Effects of solids precipitation and their mitigation. Water Resour. Res. **45**, W03402 (2009)

Roels, S.M., Ott, H., Zitha, P.L.: μ injection into brine-saturated porous media. Int. J. Greenh. Gas Control **27**, 146–154 (2014)

Schroth, M.H., Istok, J.D., Selker, J.S.: Three-phase immiscible fluid movement in the vicinity of textural interfaces. J. Contam. Hydrol. **32**, 1–23 (1998)

Shokri, N., Lehmann, P., Or, D.: Evaporation from layered porous media. J. Geophys. Res.: Solid. Earth **1978–2012**, 115 (2010)

Simjoo, M., Nguyen, Q.P., Zitha, P.L.J.: Rheological transition during foam flow in porous media. Ind. Eng. Chem. Res. **51**, 10225–10231 (2012)

Spycher, N., Pruess, K.: CO_2-H_2O mixtures in the geological sequestration of CO_2. II. Partitioning in chloride brines at $12 - 100°$ C and up to 600 bar. Geochim. Cosmochim. Acta **69**, 3309–3320 (2005)

Spycher, N., Pruess, K.: A phase-partitioning model for CO_2-brine mixtures at elevated temperatures and pressures: application to CO_2-enhanced geothermal systems. Transp. Porous Media **82**, 173–196 (2010)

Van Genuchten, M.T.: A closed-form equation for predicting the hydraulic conductivity of unsaturated soils. Soil Sci. Soc. Am. J. **44**, 892–898 (1980)

Van Hemert, P., Rudolph, E.S.J., Zitha, P.L.: Micro computer tomography study of potassium iodide precipitation in bentheimer sandstone caused by flow-through CO_2 drying. Energy Procedia **37**, 3331–3346 (2013)

Zuluaga, E., Muñoz, N., Obando, G.: An Experimental Study to Evaluate Water Vaporisation and Formation Damage Caused by Dry Gas Flow Through Porous Media. Society of Petroleum Engineers, International Symposium on Oilfield Scale (2001)